International Journal of Hydrogen Energy 257 (2026) 156397

Contents lists available at ScienceDirect

International Journal of Hydrogen Energy

journal homepage: www.elsevier.com/locate/he

Thermodynamic modelling and optimization of a 35MPa hydrogen refueling station using MATLAB-Simulink

Roberta Tatti *, Mario Petrollese

Department of Mechanical, Chemical and Material Engineering, University of Cagliari, Cagliari, Italy

ARTICLE INFO

Keywords:
Hydrogen refueling station
Hydrogen storage system
Hydrogen refueling
Heavy-duty refueling
Thermodynamic and dynamic modelling
Parametric analysis

ABSTRACT

The transport sector accounts for over 20% of global CO_2 emissions. Fuel Cell Electric Vehicles represent a promising solution for heavy-duty applications. Their deployment, however, depends on efficient Hydrogen Refueling Stations.

This study develops a thermodynamic model of a 35 MPa hydrogen refueling station for heavy-duty vehicles in Matlab-Simulink, including storage tanks, compressor, hydrogen pre-cooler, and vehicle tanks. Dynamic models are used to analyse key parameters and to assess station performance through a parametric and a realistic analysis based on bus fleet demand.

Results show that to increase number of refuelings it's necessary to increase the cascade system volume by 30% or 45%, while refueling times are between 3 and 7 min. Considering the realistic operation and a bus fleet demand, refueling time decrease to 3-4 min. Finally, the control logic for the cascade system, combined with precooling temperature of −10°C, enables safe and efficient HRS operation under variable demand conditions.

Nomenclature

Symbols			
A	Area [m^2]	ρ	Density [kg/m^3]
c	Specific heat	τ	Isobaric expansion
D	Diameter [m]	**Subscripts**	
g	Gravity acceleration [m/s^2]	C	Composite layer
h	Enthalpy [J/kg]	ext	External conditions
k	Heat transfer Coeff. [W/m^2 K]	H_2	Hydrogen
l	Length [m]	in	Initial Conditions
m	Mass [kg]	int	Internal Conditions
$\dot{m}$	Mass Flow Rate [kg/s]	L	Liner layer
MM	Molar Mass [kg/kmol]	NOM	Nominal Conditions
Nu	Nusselt number	out	Outlet conditions
p	Pressure [bar]	v	Volumetric
P	Electric Power [W]	w	Tank Wall
Q	Heat transfer [kW]	**Acronyms**	
r	Radius [m]	APRR	Average Pressure Ramp Rate
R	Ideal gas constant [J/kg K]	BEV	Battery Electric Vehicle
Ra	Rayleigh number	FCEV	Fuel Cell Electric Vehicle
Re	Reynolds number	GHG	Greenhouse Gases
s	Tank thickness	HC	Hydrogen Compressor
t	Time [h]	HG	Hydrogen Generator
T	Temperature [°C]	HPT	High pressure tank
u	Internal Energy [J/kg]	HRS	Hydrogen Refueling Station
V	Volume [m^3]	HT	Hydrogen Tank
		ICE	Internal Combustion Engine

(*continued on next column*)

(*continued*)

β	Compression ratio	LPT	Low pressure tank
γ	Temperature Coefficient [−]	NWP	Nominal Working Pressure
η	Efficiency [−]	PC	Pre-Cooling
λ	Thermal conductivity [W/m K]	SOC	State of Charge
μ	Dynamic viscosity [Pa s]	VT	Vehicle Tank

1. Introduction

In light of the continuous rise in greenhouse gas emissions in recent years, and in order to prevent global average temperatures from increasing by more than 1.5°C [1], sustainable solutions must be investigated and promoted. Particularly, the transport sector accounts for over 20% of global CO_2 emissions, with road transport as the main contributor [2].

In this context, sustainable vehicles have begun increase in recent years. Referring to electric vehicles, these are typically categorized into two main types: Battery Electric Vehicles (BEVs) and Fuel Cell Electric Vehicles (FCEVs) [2–4]. While both are emission-free during operation [2–4], they differ in how energy is stored and delivered. BEVs rely on batteries to supply electricity directly to the motor, whereas FCEVs use hydrogen, usually stored at high pressure, which is converted into electricity via fuel cells [2–4]. The choice between BEVs and FCEVs

* Corresponding author.
E-mail addresses: roberta.tatti@unica.it (R. Tatti), mario.petrollese@unica.it (M. Petrollese).

https://doi.org/10.1016/j.ijhydene.2026.156397
Received 17 March 2026; Received in revised form 29 June 2026; Accepted 2 July 2026
Available online 14 July 2026

become particularly relevant when considering the vehicle class. For light-duty vehicles, battery weight is generally manageable, and BEVs benefit from higher energy efficiency compared to FCEVs. However, in heavy-duty applications, the mass of battery systems can become a limiting factor [5–8]. Hydrogen, with its superior gravimetric energy density, allows FCEVs to maintain a lower overall system weight, making them more suitable for long-range and high-payload operations [5,7,8]. One of the key operational advantages of FCEVs is their refueling time. Light-duty FCEVs can be refuelled in approximately 3–5 min, similar to conventional petrol or diesel vehicles [5,7,8], while heavy-duty models may require around 10 min [7]. Despite these benefits, FCEVs have not yet seen widespread adoption. Current research is focused on improving the efficiency and affordability of hydrogen fuel cells, as well as expanding the infrastructure for hydrogen production, storage, and distribution. Increasing the number of refueling stations and reducing the costs associated with hydrogen logistics are considered essential steps toward broader deployment of FCEVs [9].

As the adoption of electric vehicles (both BEVs and FCEVs) continues to grow, the number of refueling stations is also increasing: in fact, the increase in Hydrogen Refueling Stations (HRS) from 2020 to 2024 has almost doubled, reaching just over 1200 units [6]. There are several types of HRS configurations: they vary depending on how the hydrogen is stored (in liquid or gaseous phase) and where it is produced (on-site or off-site). Hydrogen storage technologies can be broadly classified into three main categories: compressed gaseous hydrogen, liquid hydrogen, and material-based storage systems. Compressed hydrogen is the most widely used solution in current refueling infrastructure due to its relative technological maturity and compatibility with fast filling protocols, typically operating at 350–700 bar [9–12]. Liquid hydrogen storage enables higher volumetric energy density but requires cryogenic temperatures (−253°C), leading to significant energy penalties associated with liquefaction and boil-off management [13–16]. In contrast, solid-state storage systems, including metal hydrides and carbon-based adsorption materials, offer enhanced safety and potentially higher volumetric density, but their practical application is currently limited by thermal management constraints, slow kinetics, and system-level weight penalties [17–19]. For the storage of gaseous hydrogen, a key aspect of storage tank modelling is heating transfer during refueling. In this way, semi-empirical and empirical correlations are often used, based on dimensionless numbers such as Nusselt, Reynolds, and Rayleigh [20,21]. These allow dynamic calculation of the heat transfer coefficient, which depends on parameters like mass flow rate, injection geometry, gas temperature and pressure. The refueling of high-pressure hydrogen tanks presents significant thermodynamic challenges. Rapid gas compression and the negative Joule-Thomson effect led to a sharp temperature increase during fast fills [22–24]. This thermal rise must be carefully controlled to prevent tank deformation, material fatigue or failure. To address these risks, the SAE J2601-5 protocol, specific to heavy-duty vehicles, establishes strict safety thresholds: a maximum temperature of 85°C and a peak pressure of 1.25 times the nominal working pressure [25–27]. To ensure compliance with these limits, thermodynamic modelling of HRS systems is essential.

Numerous studies have investigated HRSs, most of them aiming to balance refueling speed with thermal safety. De Miguel et al. analysed the refueling and emptying phases of two type IV and one type III tanks at 70 MPa. Refueling times ranged from 2.6 to 9.7 min, but only one tank (19 l, type IV) achieved full State Of Charge (SOC) while meeting SAE requirements [28]. Molkov et al. proposed a thermodynamic model for two type III and one type IV tanks, but the study placed limited emphasis on SAE compliance. Final SOC values were below 100%, as pressure targets were reached before full fill [29]. Deng et al. focused on the correlation between initial and final temperatures during refueling of four tanks (two type III, two type IV), using fixed refueling times from literature (3.33–3.67 min), thus without calculating them directly [30]. Liu et al. studied both refueling and post-refueling maintenance phases, highlighting the need for preliminary cooling due to final temperatures exceeding 100°C. Refueling times were set constant at 3 and 5 min, depending on the simulation [31]. Fragiacomo et al. model the refueling of a 230 l type IV tank at 35 MPa in Matlab-Simulink, focusing on pressure losses and control valves. Refueling times varied between 3.5 and 10 min, while respecting SAE J2601-2 limits [32]. Luo et al. introduce a three-stage cascade refueling strategy, reducing refueling time from 40 to 20 min. Their Matlab-Simulink model considered both single and multiple tanks at 35 MPa [33]. Xiao et al. implemented a detailed heat transfer model for type III and IV tanks, distinguishing between hydrogen, tank wall, liner, and shell. Refueling times were around 3.5 min across various tank volumes (29–171 l) [34]. Tun et al. model the full HRS infrastructure for a 1400 l type IV tank at 70 MPa, using two configurations (28 × 50 l or 4 × 350 l). Refueling times ranged from 4.7 to 9 min, depending on SOC and temperature limits [35]. Martorelli et al. also studied a 25 l type III tank at 70 MPa, considering infrastructure components. Refueling times varied between 2 and 3.72 min [23]. Stops et al. investigated the full hydrogen lifecycle including discharge, refueling, and dormancy for gaseous, cryo-compressed, and liquid hydrogen. However, no specific refueling times were reported [36]. Saferna et al. investigated the thermodynamic behaviour during rapid filling of type IV composite tanks with hydrogen, methane, and their blends. Results showed hydrogen fills tanks 36% faster than methane but stores 28% less energy due to lower density. Hydrogen also generates 52% more entropy and reaches higher temperatures during filling [37]. Caponi et al. compared single-tank and multi-tank cascade hydrogen storage systems for refueling fuel cell buses using a dynamic thermodynamic model. Both systems delivered similar refueling time: about 38 min to dispense 37.58 kg of hydrogen per bus [38]. Galassi et al. investigated fast hydrogen filling using validated CFD simulations to assess temperature evolution and safety. Various scenarios are analysed: adiabatic, cold filling, and different pressure-rise profiles. Results showed that adiabatic filling leads to a 20% higher temperature and 10% less hydrogen mass, while cold filling reduces peak temperature by 5% and increases hydrogen mass by 3.6% [39]. Li et al. presented a thermodynamic study of fast filling in a 50 MPa hydrogen storage tank, focusing on temperature and pressure evolution. Shorter filling times result in higher temperature rise. In this regard, strategies combining pre-cooling and variable filling rates are proposed to reduce temperature and improve safety [40]. Hall and Ramasamy developed a thermodynamic model to simulate gas temperature during fast filling of hydrogen cylinder. Refueling times range from 37 to 200 s, depending on the case [41].

The most relevant results from these studies are summarized in Table 1, which highlights the key parameters and result.

The literature review highlights several gaps in the current state of research. While numerous studies have investigated the thermodynamic behaviour during hydrogen refueling, key limitations still persist. Many works do not explicitly verify compliance with SAE J2601-5 safety requirements, while others focus mainly on tank-level analyses without considering the interaction among the different subsystems composing the Hydrogen Refueling Station (HRS). Furthermore, several studies rely on prescribed refueling times rather than calculating them dynamically, or do not provide information regarding the achievable State of Charge (SOC). Most importantly, limited attention has been devoted to heavy-duty applications requiring large hydrogen capacities and repeated consecutive refueling operations.

In addition, despite the widespread adoption of cascade storage systems, most previous studies employ conventional operating strategies based on preferential depletion of the highest-pressure storage vessels, while the replenishment of downstream storage levels is generally delayed until the completion of upstream charging processes. As a consequence, the influence of alternative cascade management logics on station performance and storage utilization has received limited attention.

To address these gaps, this work proposes a fully integrated dynamic model of a 35 MPa Hydrogen Refueling Station for heavy-duty FCEV

Table 1
Studies on the thermodynamic refueling of hydrogen tanks.

Reference	Refueling time [min]	Tank type	Tank capacity [l]	Tank Pressure [MPa]
[28]	2.6 – 9.7	III	40	70
	4.2 – 4.3	IV	29	70
	4.8 – 8.1	IV	19	70
[29]	10.67	III	74	70
	7	III	40	70
	4.17	IV	29	77
[30]	3.33 – 3.67	IV	174	-
	3.33 – 3.67	III	40	77
	3.33 – 3.67	IV	29	77
	3.33 – 3.67	III	25	-
[31]	3	III	150	35
	5	IV		70
[32]	3.5 – 10	IV	230	35
[33]	17.8 – 43.3	-	90.5	35
[34]	3.5	IV	29	70
	3.5	III	171	35
	3.5	IV	72	35
	3.5	III-IV	150	35
[35]	4.9 – 9	IV	1400	70
[23]	2 – 3.72	III	25	70
[36]	-	III	500	40
	-	-		1.6
	-	III		70
[37]	1.58 – 4.67	IV	1.2 – 350	35 – 70
[38]	38	III	4030 – 6700	30 – 45
[39]	4	IV	29	70
[40]	0.2 – 3.33	-	342	55
[41]	0.62 – 3.33	III – IV	28.9 – 74.3	77.5

applications developed in MATLAB/Simulink. The model includes dedicated sub-models for the compressor, pre-cooling unit, cascade storage system, control valves and vehicle tanks, allowing the interaction among all HRS components to be evaluated under realistic operating conditions while ensuring compliance with SAE J2601-5 requirements.

Unlike conventional cascade strategies commonly adopted in literature, the present work implements an alternative storage management logic in which the replenishment of storage tanks is not postponed until the complete charging of upstream vessels. Instead, coordinated filling of different storage levels is allowed during station operation. This approach is intended to maintain favourable pressure gradients during consecutive refueling events, improve the effective utilization of the storage capacity and reduce thermal and mechanical stresses experienced by the storage tanks.

Moreover, the proposed model provides a flexible simulation framework that can be adapted to different tank technologies and operating conditions, enabling the analysis of repeated heavy-duty refueling scenarios and the assessment of the influence of key design and operating parameters on the achievable refueling capacity.

The specific objectives of this study are:

- the development of comprehensive dynamic models of a 35 MPa Hydrogen Refueling Stations to assess and optimize refueling capacity ensuring compliance with SAE J2601-5 safety protocol;
- the study of the maximum number of refuelings that the HRS is able to guarantee by varying some fundamental parameters, through a parametric analysis.

2. System configuration

This section describes the Hydrogen Refueling Station (HRS) modelled in this study, characterized by a Nominal Working Pressure (NWP) of 35 MPa. The station is designed to refuel hydrogen buses operating at 35 MPa, and the analysis focuses on assessing refueling capacity under both parametric analysis and realistic simulation while ensuring compliance with SAE J2601-5 safety protocol [42].

The system configuration is shown in Fig. 1. As shown in the figure, the HRS layout consists of several key components: a Low-Pressure Tank (LPT) for initial hydrogen storage, a Hydrogen Compressor (HC) to pressurize the hydrogen, a 3-stage cascade system of High-Pressure Tanks (HPT) for intermediate storage, a hydrogen Pre-Cooling (PC) system to manage thermal effects during refueling, Vehicle Tanks (VT, 6 per bus) and various control valves. The figure also indicates the Nominal Working Pressures of each component.

The LPT operates at 3.5 MPa, corresponding to the delivery pressure from a generic Hydrogen Generator (HG). The cascade system comprises 3 HPTs with progressively increasing pressures: 35 MPa (HPT3), 40 MPa (HPT2), and 45 MPa (HPT1). This configuration was specifically designed to enable efficient refueling of buses equipped with 35 MPa vehicle tanks. The cascade strategy allows for sequential tank utilization, optimizing hydrogen transfer and minimizing compression energy. To support this architecture, the HC is capable of compressing hydrogen to pressures up to 45 MPa, depending on which HPT is being refilled. All storage tanks (both the LPT and the HPT cascade system) are assumed to be located outdoors, exposed to ambient temperature variations throughout the year.

The purpose of the HRS is to supply high-pressure hydrogen (35 MPa) to a certain number of hydrogen buses when requested by the buses themselves. In order to understand how many buses can be refuelled without exceeding the limits set by the SAE J2601-5 protocol [27] and considering that the HRS will be refuelled with green hydrogen produced from renewable sources, a 1-h HRS working period was studied in Matlab-Simulink. This makes it possible to carry out a dynamic study of the thermodynamic behaviour inside all hydrogen tanks, particularly those on buses, to verify that the pressure and temperature values are always lower than those imposed by the protocol. Furthermore, it is possible to know how many buses can be refuelled in 1 h (always in compliance with SAE limits), leaving time at the end of the VT refueling process to refuel the storage system.

In particular, two simplifications were made during the simulation. The refueling of the vehicle tanks was assumed to occur simultaneously, meaning that all tanks were considered to experience the same inlet conditions and equivalent flow path lengths from the dispenser. Although real HRS layouts may involve small differences in pipe lengths and transient flow distribution among tanks, this simplification was adopted to focus the analysis on the overall thermodynamic behaviour of the refueling process and on compliance with SAE J2601-5 constraints. The assumption is considered acceptable for system-level investigations, where local flow distribution effects are expected to have a limited impact on the global filling dynamics.

Pressure losses associated with pipes, valves, elbows, and fittings were neglected. A preliminary assessment of typical hydrogen refueling station piping systems indicates that the resulting pressure drops are significantly smaller than both the system operating pressure level (up to 35 MPa) and the pressure variations imposed by the cascade refueling strategy. This is consistent with findings reported in the literature for similar 0D thermodynamic models of hydrogen refueling stations, where pressure drops in the piping system were found to remain below 1% of the nominal working pressure and therefore not to affect the predicted refueling operation [43]. Therefore, their influence on predicted mass flow rates and refueling time is limited at system level. However, this simplification may still lead to a slight overestimation of the effective pressure at the vehicle inlet and a corresponding underestimation of refueling duration.

Transient phenomena associated with valve switching operations and potential short-time flow instabilities are not explicitly resolved in the present 0D quasi-steady formulation. This is a common and accepted simplification in system-level thermodynamic models of hydrogen refueling: any transients generated by valve switching propagate through the system on timescales significantly shorter than the overall refueling duration and are therefore slow enough that balance-of-plant

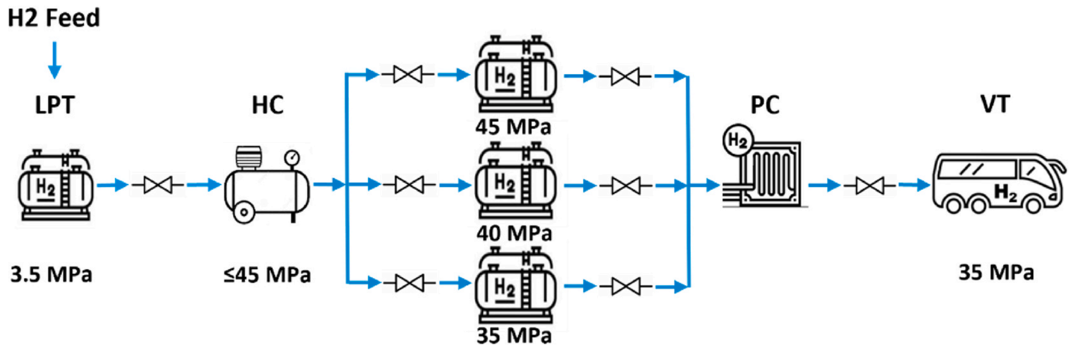

Fig. 1. Schematic system of the Hydrogen Refueling Station.

component transients can be ignored at the system level [44]. Similarly, the quasi-steady assumption implies that flow resistance and temperature variations in the piping are neglected, as their effect on the overall thermodynamic evolution is considered negligible [45]. These effects are expected to influence only local and short-duration pressure oscillations, while having negligible impact on the thermodynamic state evolution of the storage and vehicle tanks.

Finally, piping layouts and fittings strongly depend on the specific HRS design and site configuration, making a generalized and reliable estimation of distributed and localized losses difficult within a system-level modelling framework. The expected impact of these neglected phenomena on the global performance indicators remains limited and does not alter the main trends identified in this study.

3. Mathematical models

As mentioned, four main components were modelled in this study: hydrogen tanks (both storage and vehicle ones), a hydrogen compressor, different expansion valve and the hydrogen pre-cooler. All the pressure losses were neglected. In the following, the mathematical models implemented to evaluate the expected performance of each component will be described.

3.1. Vehicle tanks and hydrogen storage tanks (LPT and HPTs)

3.1.1. Vehicle tanks validation

The VTs were modelled thermodynamically and validated as reported in Ref. [46]. Starting with the conservation of mass and energy, the two balances are written in Equation (1) and Equation (2).

$$\frac{dm}{dt} = \dot{m}_{in} - \dot{m}_{out} \tag{1}$$

$$m \cdot \frac{du}{dt} + u \cdot \frac{dm}{dt} = \dot{m}_{in} \cdot h_{in} - \dot{m}_{out} \cdot h_{out} - \dot{Q}_{H_2w} \tag{2}$$

where m and $\dot{m}$ are the mass stored and the mass flow rate of hydrogen, respectively, *in* and *out* represent the refueling and emptying phases, t represent the time, u is the internal energy per unity of mass, h is the enthalpy and $\dot{Q}_{H_2w}$ represent the heat transfer from the gas to the tank wall, obtained with Equation (3).

$$\dot{Q}_{H_2w} = A_{in} \cdot k_{H_2} \cdot (T_{H_2} - T_w) \tag{3}$$

where A_{in} is the inner surface area of the tank, k_{H_2} is the heat transfer coefficient and T_{H_2} and T_w indicate the gas and wall temperature, respectively.

The heat transfer coefficient is calculated exploiting the Nusselt number (Equation (4)), expressed depending on the Reynolds number, Re, and the Rayleigh number, Ra (Equation (5)) [47].

$$Nu = \frac{k_{H_2}}{\lambda / D_{int}} = a_1 \cdot Re^{b_1} + a_2 \cdot Ra^{b_2} \tag{4}$$

$$\left[Re = \frac{4 \cdot \dot{m}}{n_{tank} \cdot \pi \cdot \mu \cdot d_{inlet}}\right] \; ; \; \left[Ra = \frac{g \cdot \tau \cdot (T_{H_2} - T_w) \cdot c_p \cdot \rho^2 \cdot D_{int}^3}{\mu \cdot \lambda}\right] \tag{5}$$

where λ is the thermal conductivity, D_{int} is the characteristic length or internal diameter of the tank (since all tanks were assumed to be positioned horizontally), a_1, b_1, a_2, b_2 are specific coefficient and exponents for the Re and Ra numbers, n_t is the total number of tanks, μ is the dynamic viscosity, D_{nozzle} is the nozzle diameter, g is the gravity acceleration, τ is the isobaric expansion coefficient, c_p is the specific heat at constant pressure and ρ is the gas density. Regarding the coefficient and exponents for the Re and Ra numbers, a_1 and b_1 were assumed equal to 0.021 and 0.67, respectively, while a_2 and b_2 are equal to 0.004 and 0.352, respectively [48]. These values were kept constant for each tank. The adopted empirical correlation, widely used in hydrogen fast-filling studies [46–48], is considered suitable for system-level dynamic simulations under high-pressure operating conditions, although local turbulence and spatial temperature gradients inside the tank are not explicitly resolved.

Solving the mass balance equation is possible to calculate the hydrogen mass inside a tank at each time step i, according to Equation (6).

$$\frac{dm}{dt} = \dot{m}_{in} - \dot{m}_{out} \rightarrow m_i = m_{i-1} + \left(\dot{m}_{in,i} - \dot{m}_{out,i}\right) \cdot \Delta t_i \tag{6}$$

Since the hydrogen mass is known, the State of Charge of the tanks, SOC_i, and the hydrogen pressure, p_i, can be calculated as reported in Equation (7).

$$\left[SOC_i = \frac{m_i}{m_{NOM}}\right] \; ; \; \left[p_i = \frac{m_i \cdot Z_i \cdot T_{H_2,i} \cdot R}{MM_{H_2} \cdot V_{tank}}\right] \tag{7}$$

where m_{NOM} is the nominal mass, Z_i is the compressibility factor (considering hydrogen a real gas), R is the gas constant, MM_{H_2} is the hydrogen molecular mass and V_{tank} is the tank volume. In particular, Z_i was calculated for each time step, considering the measured tank pressure and the average temperature of the gas calculated as reported before.

As can be seen, the hydrogen pressure depends on the temperature of the gas inside the tank, $T_{H_2,i}$, which can be found solving the energy balance (Equation (2)) and making some consideration. In fact, since $u_i = c_{v,i} \cdot T_{H_2,i}$, $h_{in,i} = c_{p,i} \cdot T_{in,i}$ and $h_{out,i} = c_{p,i} \cdot T_{out,i}$ (where c_v is the specific heat at constant volume and T_{in} is the temperature of the supplied hydrogen) it is possible to arrive at simplified relations of the variation in time of the hydrogen $\left(\frac{dT_{H_2}}{dt}\right)$ and wall $\left(\frac{dT_w}{dt}\right)$ temperatures, as indicated in Equation (8) [38,49] and Equation (10) [38], respectively. The parameters used to obtain the gas temperature (α, t^*, T^* and γ) are reported in Equation (9).

$$\left[\frac{dT_{H_2}}{dt} = (1+\alpha_i)\frac{T_i^* - T_{H_2,i}}{t_i^* + t}\right] \tag{8}$$

$$\left[\alpha_i = \frac{A_{in}\cdot k_{H_2,i}}{\dot{m}_i\cdot c_{v,i}}\right];\left[t_i^* = \frac{m_0}{\dot{m}_i}\right];\left[T_i^* = \frac{\alpha_i\cdot T_{w,i} + \gamma_i\cdot T_{in}}{1+\alpha_i}\right];\left[\gamma_i = \frac{c_{p,i}}{c_{v,i}}\right] \tag{9}$$

$$\left[\frac{dT_w}{dt} = \frac{T_{w,i} - T_{H_2,i}}{t_{w,i}^*}\right];\left[t_{w,i}^* = \frac{m_w\cdot c_{p,w}}{A_{in}\cdot k_{H_2,i}} = \frac{\rho_w\cdot V_{tank}\cdot c_{p,w}}{A_{in}\cdot k_{H_2,i}}\right] \tag{10}$$

where m_0 is the initial hydrogen mass inside the tank, γ is the ratio between the specific heat at constant pressure and volume, m_w is the mass of the tank, calculated multiplying the tank density (ρ_w) and volume (V_{tank}), and $c_{p,w}$ is the specific heat of the wall tank. The hydrogen gas temperature is modelled as a spatially lumped, time-dependent average state, meaning that no spatial temperature gradients within the gas phase are resolved. This assumption is consistent with zero-dimensional thermodynamic models commonly used for fast-filling simulations [48].

Since the type III and IV tanks are characterized by two materials, the calculation of the wall temperature has been discretized, considering the increasing of the area (A_j) and volume (V_j) of the tank wall, as indicated in Equation (11) and Equation (12), respectively. In particular, it was assumed to consider 10 shell elements for each layer, each one with the same length dx [48].

$$A_j = 2\cdot\pi\cdot\left[(r+(j-1)\cdot dx\right]\cdot l_{int} + 4\cdot\pi\cdot\left[(r+(j-1)\cdot dx\right]^2 \tag{11}$$

$$V_j = \pi\cdot\left[(r+j\cdot dx)^2 - (r+(j-1)\cdot dx)^2\right]\cdot l_{int} + \frac{4}{3}\cdot\pi\cdot\left[(r+j\cdot dx)^3 - (r+(j-1)\cdot dx)^3\right] \tag{12}$$

where r is the inner radius of the tank, L_{int} is the total internal length of the tank and j indicates the tank layer. The discretization of the wall temperature, as reported in Equation (13), was implemented with different parameters (from x_1 to x_6). Depending on the layer, indexed in the first column of Table 2, it is possible to substitute each parameter in Equation (13) to obtain the formula for each layer considered. The subscript L indicates the liner layer (aluminium), while the C the composite one (carbon fibre reinforced polymer).

$$\frac{dT_{w,j}}{dt} = \frac{A_j\cdot x_1\cdot\left(x_2 - T_{w_j}\right) - A_{j+1}\cdot x_3\cdot\left(T_{w_j} - x_4\right)}{x_5\cdot x_6\cdot V_j} \tag{13}$$

In particular, the first term in the numerator of Equation (13) considers the heat exchanged due to the hydrogen mass flow. Therefore, during filling operations ($\dot{m} > 0$) it influences the temperature increase, while during unloading operations ($\dot{m} < 0$) it determines a temperature decrease. In stand-by conditions (no mass flow), this contribution has been neglected and the evolution of the wall temperature has been calculated considering only the second term, which represents the heat exchange between the tank wall and the surrounding environment. In these conditions, in fact, the gas temperature remains approximately constant, while the wall temperature tends to approach thermal equilibrium with the ambient temperature.

All the values dependent on the gas pressure and temperature, as c_p c_v, μ, h, u, λ, τ and ρ were obtained by Coolprop, as a function of pressure and temperature, at each time step.

The main parameters of the VT validated, such the geometry and material properties, are reported in Table 3.

In particular, only 2 cases were analysed and validated of the 3 reported in the reference study (due to data availability) [48]: Test no. 4 and Test no. 12. The characteristics of these tests, as well the initial simulation data, are reporter in Table 4.

To evaluate the error between the experimental values and the ones calculated with the Matlab- Simulink model, the Root Mean Square Error ($RMSE$) and its percentage value, compared to the average of the experimental values ($RMSE_{\%}^{MEAN}$), were calculated with Equation (15).

$$\left[RMSE = \sqrt{\frac{1}{n}\sum_{i=1}^{n}(y_i - \hat{y}_i)^2}\right];\left[RMSE_{\%}^{MEAN} = \frac{RMSE}{\frac{1}{n}\sum_{i=1}^{n}y_i}\cdot 100\right] \tag{15}$$

where n indicates the number of measurement data, y_i are the experimental values and $\hat{y}_i$ are the results calculated with the model at each time step. The results are summarized in Table 5.

As can be noted, the percentage error is always lower than 1% for both pressure and temperature. Regarding the absolute error for temperature, this is just a bit lower or greater than 2.5 K, depending on the test, while for pressure the values are very low and included between ~0.05 and ~0.07 MPa.

Given that the error results fall within acceptable limits, the validated model of the VT was adopted as the basis for the modelling of both low- and high-pressure storage tanks.

3.1.2. Hydrogen tanks considered in this study

The LPT and HPT considered are a type I and a type IV tank, respectively, with the first modelled from data from Ref. [49], while the VTs are type III tank, as the tank validated before. As reported previously, the VTs are 6, accordingly with the hydrogen bus chosen for this study [50].

The different types of tanks were modelled with the same principles used for the VT validation (from Equation (1) to Equation (13)). Since no experimental data are available for this specific study, the increase in VT pressure during the refueling phase was calculated considering a constant Average Pressure Ramp Rate (APRR), as given in Equation (14).

$$p_{VT,i} = p_{VT,(i-1)} + APRR\cdot t_i \tag{14}$$

where $p_{VT,i}$ and $p_{VT,(i-1)}$ are the gas pressure at time t_i and $t_{(i-1)}$, respectively. The APRR is defined as the average rate of pressure increase in the vehicle tank during refueling (MPa/min), and it is used as a control parameter to regulate the hydrogen filling process in accordance with the SAE J2601-5 protocol. The hydrogen mass inside the VT was

Table 2
Parameters used to calculate the discretized wall temperature.

	x_1	x_2	x_3	x_4	x_5	x_6
$j = 1$	$k_{H_2,i}$	T_{H_2}	λ_L/dx_L	$T_{w_{j+1}}$	ρ_L	c_{p_L}
$1 < j < 10$	λ_L/dx_L	$T_{w_{j-1}}$	λ_L/dx_L	$T_{w_{j+1}}$	ρ_L	c_{p_L}
$j = 10$	λ_L/dx_L	$T_{w_{j-1}}$	$\frac{\lambda_L + \lambda_C}{dx_L + dx_C}$	$T_{w_{j+1}}$	ρ_L	c_{p_L}
$j = 11$	$\frac{\lambda_L + \lambda_C}{dx_L + dx_C}$	$T_{w_{j-1}}$	λ_C/dx_C	$T_{w_{j+1}}$	ρ_C	c_{p_C}
$11 < j < 20$	λ_C/dx_C	$T_{w_{j-1}}$	λ_C/dx_C	$T_{w_{j+1}}$	ρ_C	c_{p_C}
$j = 20$	λ_C/dx_C	$T_{w_{j-1}}$	$k_{H_2,out}$	T_{amb}	ρ_C	c_{p_C}

Table 3
Properties of the VT tank validated [48].

Parameter		VT (type III)	Parameter		VT (type III)
$p_{in} - p_{nom}$	[MPa]	2.99 – 35	D_{nozzle}	[mm]	6
$m_{in} - m_{nom}$	[kg]	0.779 – 7.68	$\lambda_l - \lambda_C$	[W/mK]	202 – 1
V_{tank}	[m^3]	0.32	$\rho_l - \rho_C$	[kg/m^3]	2700 – 1494
$D_{int} - D_{ext}$	[m]	0.337 – 0.417	$c_{p,l} - c_{p,C}$	[J/kgK]	900 – 938
$L_{int} - L_{ext}$	[m]	3.05 – 3.13	k_{out}	[W/m^{2}K]	8
Tank Thickness – dx	[m]	0.04 – 0.002			

Table 4
Initial data for Test no. 4 and Test no. 12 simulations [48].

		Test no. 4	Test no. 12
Pressure ramp rate	[bar/min]	50	100
Pre-cooling	[°C]	−40	0
Ambient temperature	[°C]	15	15
Starting gas temperature	[°C]	15.06	15.35
Starting gas pressure	[bar]	30.32	29.47
Starting gas mass	[g]	801.56	778.71
Starting gas density	[kg/m^3]	2.505	2.433

Table 5
Error results for Test no. 4 and Test no. 12.

	Test no.4		Test no. 12	
	RMSE	$RMSE_{\%}^{MEAN}$	***RMSE***	$RMSE_{\%}^{MEAN}$
Pressure	0.0731 MPa	0.438%	0.0514 MPa	0.316%
Temperature	2.682 K	0.87%	2.468 K	0.766%

then calculated by multiplying the tank volume and density (obtained with Coolprop as a function of pressure and temperature), while the mass flowrate is a result of Equation (6), since the mass is known.

Since the mass flowrate required by the VTs is known, this value was used to empty the HPT cascade system. In particular, the emptied HPT depends on the pressure inside both tanks (HPT and VT). Logically, the first HPT to be emptied is the one at 35 MPa, while the last one is the 45 MPa tank. Since the mass flow of the HPTs is known, all other parameters can be calculated.

The LPT was modelled similarly to the HPT modelling, considering in this case the compressed hydrogen as mass flow rate to refuel the cascade system. Furthermore, since Type I tanks are characterized by a single material, the discretization of the tank wall temperature in Equation (13) was calculated differently. In particular, only 3 discretization steps of Table 2 for the individual layers are considered: the first ($j=1$), the second (with $1<j<20$, where λ, ρ, c_p and dx are the same for each layer), and the last one ($j=20$). All other parameters were calculated similarly to the other tank types.

The main parameters of the tanks considered in this study are reported in Table 6. Regarding geometries, all tank types were scaled starting from data reported in Ref. [46].

The nominal pressure of the LPT is equal to the hydrogen production pressure in the HG, while that of the HPT cascade system is able to refuel the VT at 35 MPa. The three-stage cascade configuration (HPT1 at 45 MPa, HPT2 at 40 MPa, and HPT3 at 35 MPa) was selected as the optimal balance between refueling efficiency and system complexity [51]. Previous studies demonstrated that 3 to 4 tanks represent the optimal configuration for cascade systems, as adding more than 4 tanks yields energy savings of less than 4% per additional tank [51]. A 2-tank cascade would result in excessive pressure drops and longer refueling times, particularly in the final phase when the VT approaches 35 MPa, as insufficient pressure differential significantly reduces mass transfer rates [38]. Conversely, a 4-tank system would provide only marginal improvements while significantly increasing capital costs, space requirements, and maintenance complexity [51].

The chosen 3-stage configuration with approximately 5 MPa pressure steps ensures adequate pressure differentials throughout the refueling process, maintaining sufficient mass flow rates. Research showed that transitioning from a 1-tank to a 3-tank cascade system reduces total energy consumption by approximately 30-34% [51,52], while the cascading approach optimizes station storage management by minimizing pressure differentials between refueling and refuelled tanks throughout the process [38]. This pressure gradient allows approximately 70-80% of the hydrogen stored in each HPT to be effectively transferred to the downstream tank before pressure equalization limits further transfer, thus maximizing the useable capacity of each vessel [53]. Regarding the dimensions, the total volume of the 6 VTs was obtained to contain in total 35 kg of hydrogen, nominal quantity of hydrogen storable in the bus chosen [50].

Table 6
Characteristic of the different tank types considered.

Parameter		LPT	HPT1	HPT2	HPT3	VT
Type		I	IV	IV	IV	III
p_{nom}	[MPa]	3.5	45	40	35	35
m_{nom}	[kg]	425.32	36.03	39.46	41.39	5.83
V_{tank}	[m^3]	150	1.25	1.5	1.75	0.27
D_{int}	[m]	2.689	0.693	0.737	0.776	0.328
D_{ext}	[m]	2.856	0.757	0.805	0.847	0.406
l_{int}	[m]	24.17	2.849	3.028	3.188	2.97
l_{ext}	[m]	24.5	2.913	3.096	3.259	3.05
AR	[−]	8.58	3.85	3.85	3.85	1.24
s	[mm]	83.5	32	34	35.5	39
dx	[mm]	4.175	1.6	1.7	1.775	1.95
d_{inlet}	[mm]	10.8	5.4	5.4	5.4	6
λ_L	[W/mK]	50	0.3	0.3	0.3	202
ρ_L	[kg/m^3]	7850	1050	1050	1050	2700
$c_{p,L}$	[J/kgK]	490	1700	1700	1700	900
λ_C	[W/mK]	50	0.43	0.43	0.43	1
ρ_C	[kg/m^3]	7850	1560	1560	1560	1494
$c_{p,C}$	[J/kgK]	490	1102	1102	1102	938
$k_{h,outer}$	[W/m^{2}K]	100	100	100	100	8

3.2. Hydrogen compressor

The HC considered in this study is a volumetric compressor (continuously operating with variable load and pressure), which has been modelled to avoid a final temperature after compression above 135°C [54] with the same principles indicated in Ref. [46]. Considering a gas inlet temperature always equal to 15°C (due to an intercooler before each stage), a minimum pressure of 1.5 MPa (allowing LPT to discharge in a range between 1.5 MPa and 3.5 MPa), and the maximum pressures required by the HPTs, it is necessary to have at least 3 stages. The average compression ratio for a final pressure of 35 MPa, 40 MPa and 45 MPa, $\beta_{(k)}$, are equal to 2.86, 2.99 and 3.11 respectively.

Fig. 2 shows a simplified scheme of a generic stage k, with all parameters calculated before or after the stage (indicate as HC(k)) and the intercooler (IC(k)).

Starting from the initial conditions of pressure and temperature (before the first stage) it is possible to define enthalpy (h) and entropy (s) with Coolprop. The conditions in the middle of the first stage were obtained considering constant entropy and intermediate pressure, through which the isentropic temperature and the isentropic enthalpy ($h_{is(k)}$) were calculated. These last values were then used to find the stage outlet enthalpy ($h_{(k)}$), as a function of the isentropic efficiency (Equation (14), valid for compression ratios between 1.1 and 5 [55]), and the outlet temperature ($T_{(k)}$) with Coolprop.

$$\eta_{is(k)} = 0.1091 \cdot (\ln \beta_{(k)})^3 - 0.5247 \cdot (\ln \beta_{(k)})^2 + 0.8577 \cdot \ln \beta_{(k)} + 0.3727 \quad (14)$$

As mentioned, an intercooler was modelled at the end of each stage to keep the outlet temperature equal to 15°C. The same approach was adapted for all stages. At the end of each stage, it is possible to calculate the power needed (Equation (15)), while by adding the power of each stage the total power of the compressor can be obtained.

$$P_{(k)} = \frac{W_{(k)}}{\eta_{is(k)} \cdot \eta_{v(k)}} = \frac{\dot{m}_{H_2} \cdot (h_{(k)} - h_{(k-1)})}{\eta_{is(k)} \cdot \eta_{v(k)}} \quad (15)$$

where $W_{(k)}$ is the work of a generic stage and $\eta_{v(k)}$ is the stage volumetric efficiency, calculated with Equation (16) (Smith, 2005).

$$\eta_{v(k)} = 1 - \beta_{(k)} - c \cdot \left(\frac{Z_{in}}{Z_{out}} \cdot \beta_{(k)}^{1/\gamma} - 1 \right) \quad (16)$$

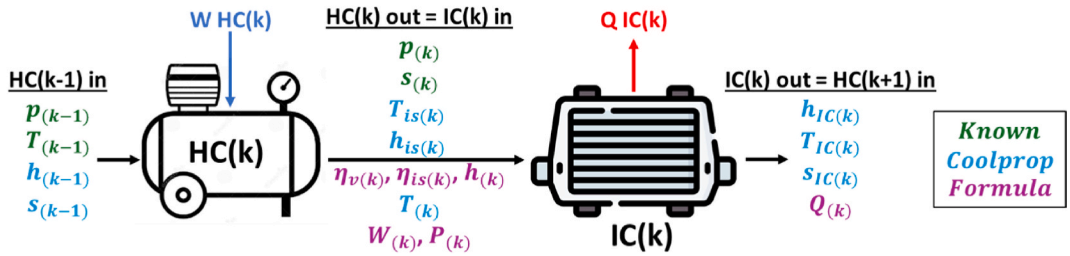

Fig. 2. Simplified scheme for a compressor stage.

where c is the cylinder clearance (assumed equal to 10%) and Z_{in} and Z_{out} are the compressibility factors at the inlet and outlet conditions considering all stages, respectively. It is worth noting that the compressor is not modelled with a constant efficiency. Instead, the isentropic efficiency (Equation (14)) and the volumetric efficiency (Equation (15)) are evaluated at each stage as a function of the compression ratio β(k). Therefore, the compressor performance varies with operating conditions and load, allowing the model to capture changes in energy consumption under different pressure levels.

3.3. Expansion valve and hydrogen precooling

The expansion valve located between the HPT cascade system and the VT have the important role of regulating the pressure between the two mentioned components to keep the APRR constant. During the expansion process two simplifications were adopted: 1. the heat exchanged with the environment is zero (adiabatic process) and 2. the variation of kinetic energy is zero. This means that the enthalpy remains constant. These considerations help to find the valve outlet temperature, or the inlet temperature of the VTs. In fact, since the HPT and VT pressures are known, as well as the temperature of the HPT, it is possible to find the required temperature.

Regarding hydrogen pre-cooling, this was modelled with the same equation used in HC intercooling to calculate heat removal from hydrogen. Since the mass flow rate at the VT inlet is known, along with the enthalpy and inlet pressure (which vary depending on the HPT tank emptying) and the desired final temperature to which the hydrogen must be cooled, the outlet enthalpy was obtained. The heat to be removed from the gas was then calculated by multiplying the mass flow rate by the enthalpy difference between the initial and final states. Regarding electrical energy consumption, since the hydrogen cooling temperature per SAE J2601-5 ranges from −40°C to 0°C, different Coefficients of Performance (COP) were considered depending on the cooling temperature, as reported in Table 7 [56]. The electrical power of the cooler was therefore obtained by dividing the thermal power Q by the COP.

3.4. Strategy management and control logic for the hydrogen refueling station

The HRS management strategy was designed to determine the maximum number of buses that can be refuelled within 1 h. A 2-min pause between consecutive refueling events was assumed, while each refueling process was modelled in compliance with the SAE J2601-5 protocol limits for pressure and temperature. Considering a theoretical capacity of the HRS, at the start of each simulation each VT was considered to be refuelled from 10% to 100% SOC, whereas the LPT and HPT were assumed to be fully charged (SOC = 100%).

Table 7
Different COP for hydrogen cooling temperature.

Cooling T [°C]	−40	−30	−20	−10	0
COP	1.95	2.2	2.55	3	3.4

The methodology used to calculate all the HRS outputs is represented in Fig. 3, which highlight the most relevant output calculated for each block modelled with Matlab-Simulink.

The key output of each VT simulation is the mass flow rate requested by each of the six VTs, which is identical, and calculated as a function of the APRR. This flow rate is essential to determine the overall outflow from the HPT cascade system, equal to the sum of the mass flow rates requested by all VTs. Specifically, hydrogen is discharged from the HPT whose pressure is higher than that of the VT being refuelled. Since at the beginning of the simulation the VTs are nearly empty and all HPTs are fully charged, priority is given to the HPT with the lowest pressure, i.e., HPT3 (35 MPa), followed by HPT2 and HPT1 in order of increasing pressure. It is also assumed that cascade switching between storage tanks occurs instantaneously and under ideal control conditions, without considering actuator delays or control system dynamics. In practice, such effects may introduce minor transient deviations in mass flow distribution; however, their influence is expected to be limited at system-level analysis.

To maximize the number of buses that can be refuelled in 1 h, a parallel refueling logic for the HPT cascade system was implemented. The HPT logic is represented in Fig. 4, where *i-1* highlights the priority of HPT3.

In particular, whenever a tank in the cascade is not discharging, it is refilled if its SOC is below 100%. Again, priority is given to the tank with the lowest pressure, i.e., HPT3. Finally, at the end of the 1-h period, a final refueling is carried out so that the cascade system is restored to its initial condition (SOC = 100%). Within this management logic, both the HPT tank selected for discharge and the corresponding mass flow rate (during discharging and refueling phases) and the compression pressure, depending on which HPT tank is being refilled, are determined. Transient pressure fluctuations and flow instabilities associated with valve switching operations are not explicitly modelled, as the system is treated under a quasi-steady-state assumption at each time step. Therefore, the model captures the overall mass and energy balances, while neglecting fast hydraulic transients that may occur during valve actuation.

Other key parameters derived from calculations within the VT and hydrogen storage system include pressure, gas and wall temperatures, mass and SOC. Given the pressure and temperature values of the HPT cascade system and the pressure of the VTs, it is possible to compute the outlet temperature at the valves located downstream of the cascade system.

Moreover, depending on which valve is active (based on the hydrogen flow from the HPT currently being discharged) it is possible to determine the amount of heat that must be removed from hydrogen during the cooling phase, as well as the corresponding electrical consumption, as previously described.

Similarly, the mass flow rate of the LPT has been calculated. During the discharging phase, this mass flow rate matches the demand from the HPT cascade system. In particular, the HC compresses the hydrogen to the pressure required by the active HPT. Differently from the cascade system, the LPT is refuelled with hydrogen produced by the HG during all day (if its SOC is lower than 100%), considering hydrogen production at nominal power. Thus, the target number of VTs is refuelled every hour, while the cascade system is refuelled during and after the VT

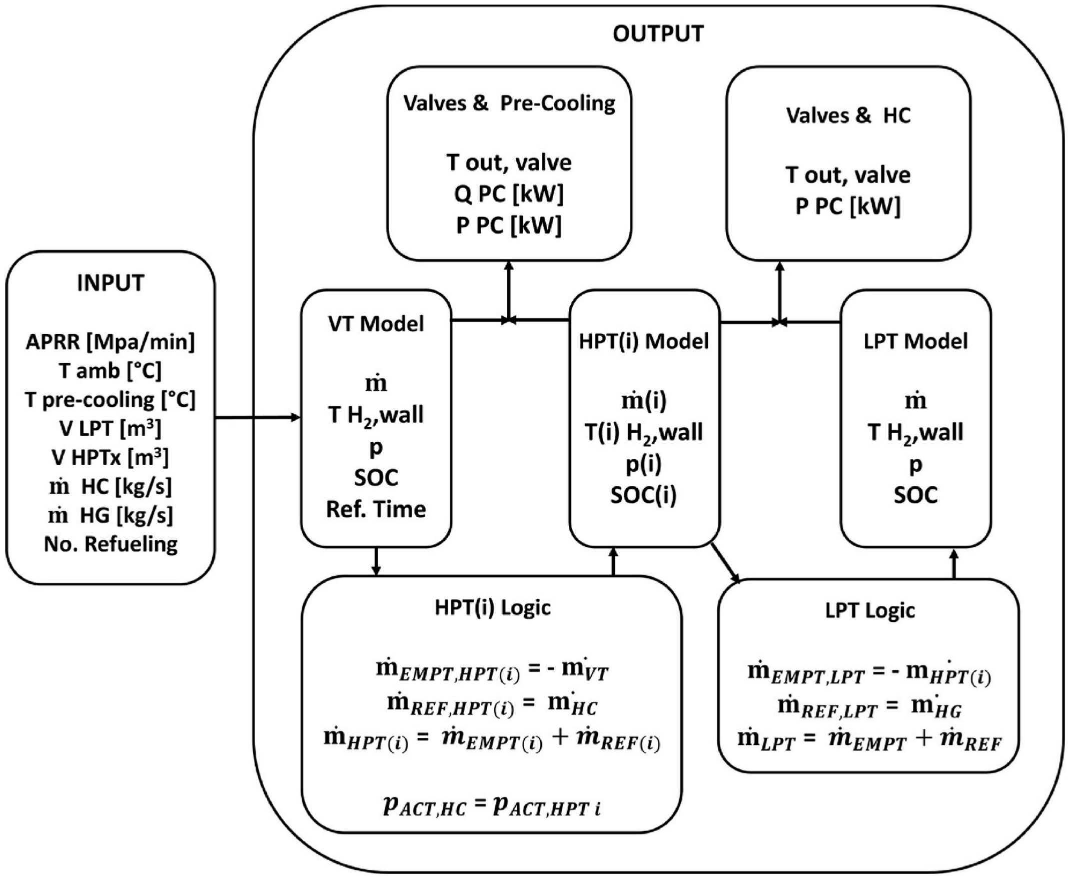

Fig. 3. HRS output calculation logic.

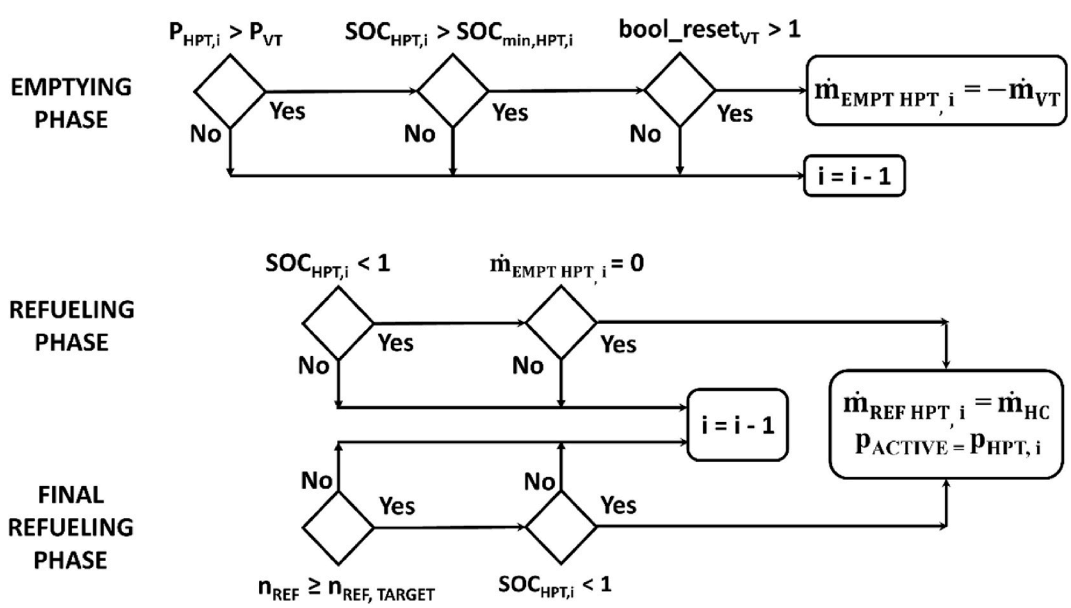

Fig. 4. HPT cascade system control logic.

refueling. The LPT is refuelled hourly at the nominal HG production and emptied when required by the buses.

With all relevant parameters known for the LPT, it is also possible to calculate the outlet temperatures at the valves located upstream of the cascade system and at the valve between the LPT and the HC.

It should be noted that the validation is performed at the component level, focusing on the vehicle tank, which governs the thermodynamic behavior during refueling. System-level outputs such as refueling time are not directly validated against experimental data, as they depend on the implemented refueling protocol (SAE J2601-5) and operating conditions, and are therefore treated as model predictions. Experimental validation of the complete HRS and of the implemented cascade management strategy would require full-scale station measurements under controlled operating conditions, which are currently scarcely available in the open literature, especially for heavy-duty 35 MPa applications.

4. Results and discussion

This section reports the results obtained from the thermodynamic model and analysis of the 35 MPa Hydrogen Refueling Stations, to assess and optimize refueling capacity under different operational scenarios while ensuring compliance with SAE J2601-5 safety protocol. A parametric analysis is carried to identify optimal initial conditions that maximize consecutive refueling in 1 h (5 ÷ 8 refueling with 3 ÷ 7 min refueling times).

4.1. HRS thermodynamic model results

The results obtained from the HRS thermodynamic model were achieved using the methodology represented in Fig. 3. In particular, several simulations were conducted to identify the inputs capable of ensuring the desired SOCs (100% for VT and HPT cascade system) and the temperature and pressure limits imposed by SAE J2601-5 protocol with low energy consumptions. Among these inputs, the APRR plays a key role, as it directly governs the refueling dynamics and was therefore selected and tuned to meet the target operating conditions. The inputs, indicated as base case, are reported in Table 8.

As indicated in the table, a target number of 5 hourly refueling was selected. The tank volumes are those indicated in Table 6, which also reports the geometric and material characteristics. As previously reported, the VT starts from an SOC of 10%, while the storage tanks are completely full at the beginning of the simulation. An ambient temperature of 20°C was chosen, while hydrogen is supplied at a temperature of −10°C. The mass flow rate required by the VT is influenced by the required APRR, set at 4.5 MPa/min, while the compression and hydrogen production mass flow rates were initially selected as 60 g/s and 14.59 g/s respectively. In particular, the hydrogen production value of 14.59 g/s was selected based on the bus demand considered in this case study, which will be explained subsequently. This mass flow rate is capable of refueling the LPT and bringing it back to an SOC of 100% at the end of a working day, always ensuring the hydrogen required by the buses during their respective refueling hours. With these values, it is possible to reach the desired number of refueling without exceeding the pressure and temperature limits, while also ensuring the refueling of the cascade system within 1 h. The main results, obtained at the end of the simulation, are visible in Table 9.

As just mentioned, the final number of refuelings equals the desired value of 5. With the considered APRR each refueling takes just over 7 min in total, for a total of approximately 45 min dedicated to vehicle refueling (considering a 2-min pause between consecutive refuelings). This means that the final SOC of each VT is 100%, as well as the HPT cascade system tanks are also completely refuelled by the end of the hour. Regarding the LPT, this tank is refuelled up to 100% throughout the day. The maximum flow rate delivered by the dispenser is 83.26 g/s, which is uniformly distributed among the 6 VTs present in one bus.

The pressure limit is respected in every tank, based on the limit imposed by the J2601-5 standard at a value equal to 25% above the nominal working pressure (1.25•NWP). These limits are, specifically, 43.75 MPa for the VT and HPT3, 56.25 MPa for HPT1, 50 MPa for HPT2, and 4.375 MPa for the LPT. From the results, it can be observed that the final pressure value of the VT is slightly lower than the nominal value, while in the other tanks the value is slightly higher or equal, but still within the limits. This difference is due to the different pressure calculation for the VT, set as a function of the APRR, and for the storage tanks, for which the pressure is obtained as a function of the ideal gas equation, depending on the established mass flow rates in the downstream tanks. Furthermore, the nominal value is exceeded due to the mass increase inside the tank, and consequently the temperature increase.

The temperature limit of 85°C is also not exceeded. The tank that comes closest is the HPT3, which is the most stressed during the vehicle refueling phase and during the refueling phase through compressed hydrogen, reaching a value of approximately 74°C.

Regarding power of HC and Pre-Cooling, the first reached a maximum power of almost 450 kW, while the second reached only 32.72 kW, which is 7.27% of the compressor. The energy consumption values were obtained integrating the power over the considered hourly interval: the results are 287.24 kWh and 11.55 kWh for the HC and PC, respectively.

Considering a total of approximately 175 kg of hydrogen delivered per hour (5 refuelings of 35 kg each), the specific energy consumption is about 1.64 kWh/ kg_{H_2} for compression and 0.066 kWh/ kg_{H_2} for pre-cooling. These values are consistent with literature data, where compression typically represents the dominant contribution (on the order of 2–5 kWh/kWh/ kg_{H_2}) [57,58], while pre-cooling has a significantly lower impact (generally below 0.1–0.3 kWh/kWh/ kg_{H_2}) [57,59].

In the following, the graphical results of the trends of the most relevant parameters (mass flow rate, SOC, pressure and temperature) for all tanks are reported, as well as the consumption and parameters of the HC and PC.

Table 8
Input for HRS model – Base Case.

Parameter		Value	Parameter		Value
APRR	[MPa/min]	4.5	N. Ref Target	[−]	5
T Amb	[°C]	20	T Pre-Cooling	[°C]	−10
SOC VT	[%]	10	V VT	[m^3]	0.27
SOC HTP$_{1,2,3}$	[%]	100	V HPT$_{1,2,3}$	[m^3]	1.25/1.5/1.75
SOC LPT	[%]	100	V LPT	[m^3]	150
MF HC	[g/s]	60	MF HG	[g/s]	14.59

Table 9
Results obtained from the base case simulation.

Parameter		Value	Parameter		Value
Ref. Time	[min]	7.15	No. Ref.	[−]	5
Max p VT	[MPa]	34.79	Max T H_2 VT	[°C]	51.05
Max p HTP1	[MPa]	47.12	Max T HTP1	[°C]	33.63
Max p HTP2	[MPa]	44.3	Max T HTP2	[°C]	49.93
Max p HTP3	[MPa]	41.69	Max T HTP3	[°C]	73.53
Max p LPT	[MPa]	3.5	Max T LPT	[°C]	20
SOC VT	[%]	100	SOC HTP$_{1,2,3}$	[%]	100
SOC LPT	[%]	72.31	Max MF Disp.	[g/s]	83.26
Max HC Power	[kW]	448.4	HC Consumption	[kWh]	287.24
Max PC Power	[kW]	32.72	PC Consumption	[kWh]	11.55

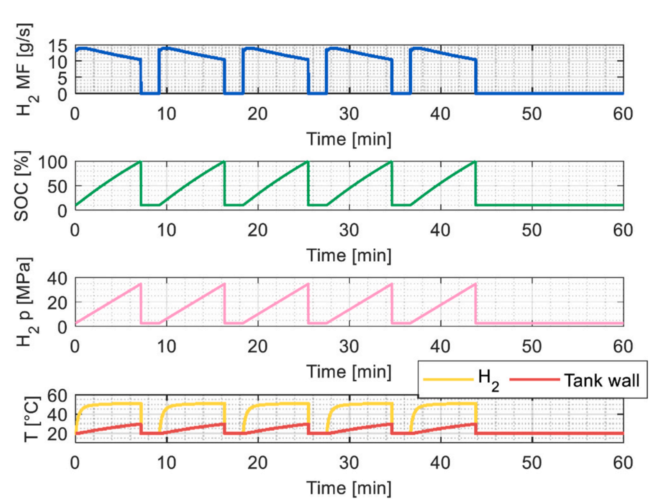

Fig. 5. Mass Flow, SOC, pressure and temperature of the VT (base case).

4.1.1. Vehicle tanks results

Fig. 5 presents the VT results obtained from the thermodynamic model of the HRS. The figure shows, from top to bottom, the trends of mass flow rate, SOC, pressure and gas and wall temperatures.

The mass flow rate trend is typical of refueling with a constant APRR and results from two competing thermodynamic effects. Initially, the mass flow rate increases rapidly due to the greater pressure difference between the HPT cascade system and the VT, which drives hydrogen transfer. However, as refueling progresses, the compression of hydrogen inside the VT causes a significant temperature increase due to the Joule-Thomson heating effect and compression work. This temperature increase reduces the hydrogen density inside the tank, which in turn increases the internal pressure more rapidly than would occur in an isothermal process. Consequently, the pressure differential between the source and the VT decreases faster, leading to a reduction in mass flow rate. The interplay between these two effects, pressure-driven mass transfer (which dominates initially) and temperature-induced pressure rise (which dominates later), determines the characteristic declining mass flow rate profile observed during the refueling process. As the VT pressure approaches that of the active HPT in the cascade, the mass flow rate diminishes until the system switches to the next lower-pressure HPT to continue refueling.

As assumed by the logic, after refueling a vehicle, a 2-min pause begins, during which all the most important parameters are reset. At each refueling, the SOC of each VT starts from 10% to reach a full charge of 100% in approximately 7 min, as previously reported. The pressure trend is analogous to that of the SOC, with the maximum value reached close to the nominal conditions.

Regarding temperatures, the initial value is equal to that of the ambient temperature (20°C), while the temperature of the hydrogen delivered by the dispenser is close to that set in the PC, equal to −10°C. The highest value reached by the temperature of hydrogen is approximately 51°C. The temperature trend is similar to those of the mass flow rate, characterized by a high increase at the beginning, followed in this case by a more contained increase until the end of the refueling. This rapid temperature increase at the beginning is due to the low initial pressure and the Joule-Thomson effect. In fact, hydrogen has a negative Joule-Thomson coefficient for the considered temperatures, which means that a free expansion heats it instead of cooling it. The wall temperature assumes lower values instead, with a maximum of approximately 5°C, with an increasing trend.

4.1.2. HPT cascade system results

The results of the cascade system control logic are represented in the following figures. Each figure indicates, as already done for the VT, the trends of mass flow rate, SOC, pressure and temperature starting from HPT3, at the top, down to HPT1, at the bottom.

Fig. 6 shows the mass flow rate trend. As previously reported, the VT is refuelled by the cascade system tank characterized by a pressure higher than that of the VT itself. The emptying priority is perfectly visible in the figure: initially the VT is filled with hydrogen from HPT3 (characterized by an initial negative mass flow rate), after which HPT2 and HPT1 are emptied. This trend is repeated for all refueling, as visible. Regarding the tank filling logic, HPT3 begins to refuel with compressed hydrogen simultaneously with the emptying of HPT2 (with a mass flow rate equal to that of compression), just as HPT2 begins to refuel as soon as HPT1 starts to empty. Finally, HPT1 refuels during the emptying of HPT3. From the graph, the final filling of each tank can also be observed, which occurs once the desired number of vehicle refueling is completed (after approximately minute 42). Finally, given the logic set with priority to HPT3 both in the filling and emptying phases, it is possible to observe that this tank is the most used among the three, while for the same reasons HPT1 is the least used.

Fig. 7 shows the gas and wall temperature trends for each HPT. Looking at the temperature trends for HPT3, at the beginning both temperatures are characterized by a slight decrease, due to the first

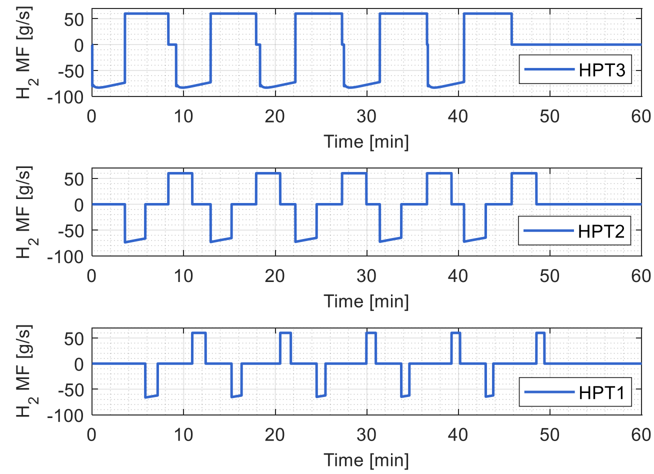

Fig. 6. Mass Flow of the HPT3, HPT2 and HPT1 (base case).

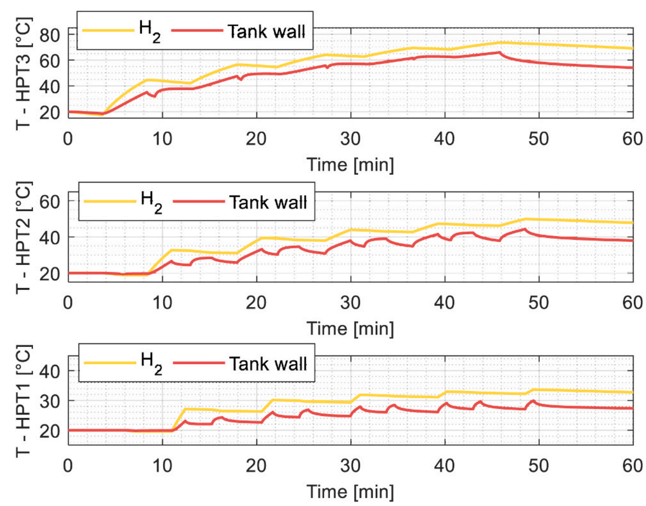

Fig. 7. Temperature of the HPT3, HPT2 and HPT1 (base case).

emptying phase of the tank. This is followed by an increase in both temperatures, with the gas temperature reaching a slightly higher value. These two phases are followed by a brief pause, also visible in the mass flow rate graph: in this phase, the gas temperature decreases in a very contained and almost imperceptible way, while the wall temperature decreases more evidently, although slightly, trying to reach equilibrium with the ambient temperature.

This temperature decrease leads to the subsequent emptying phase, during which the gas temperature decreases, causing an increase in the wall temperature. The observed phenomenon can be explained considering the thermal inertia and energy exchange between gas and tank walls. When the subsequent emptying phase begins, the pressure decrease causes the gas to cool due to expansion, while the walls are now heated by the gas flow which, although colder, creates turbulence and favours heat exchange from the environment toward the walls. In the subsequent phases, characterized by continuous filling and emptying, both temperatures follow the same trend: they increase during refueling and decrease during emptying. In the final phase, with no flow rate and therefore at rest, both temperatures decrease, with the walls releasing more heat to the outside compared to the temperature released by the gas.

The same trend occurs in HPT2. This tank presents an initial pause phase, followed by emptying, with consequent decrease of both temperatures in a very contained manner. At this point there is another pause, during which the difference in both temperatures is almost imperceptible (before minute 10). This is followed by the first filling, which instead causes a more evident temperature increase, with the gas reaching higher temperatures. Subsequently, another pause occurs, during which the gas slightly decreases its temperature, against a greater decrease in wall temperature. At the next emptying, as already observed, the gas temperature decreases, while that of the walls increases.

HPT1 is also characterized by a similar trend. In summary, it can be said that in the initial phase, when a tank has not yet undergone a filling phase, the differences in both temperatures are hardly visible. The filling phases can instead be identified by the 5 upward peaks of the gas temperature, followed by an increase in wall temperature. The post-filling pause phases are visible from the downward elbows of the wall temperature, more or less evident depending on the duration of the pause. Finally, the emptying phases are characterized by opposite temperature behaviour: that of the gas decreases, while that of the walls increases.

Ambient temperature variations are expected to affect the thermal behaviour of the HRS and the effectiveness of the pre-cooling system. In particular, higher ambient temperatures may increase the overall thermal load on the system, making deeper pre-cooling more beneficial for limiting gas temperature rise during refueling. Conversely, under colder ambient conditions, the thermal response of the storage system during consecutive refueling operations may differ due to changes in heat exchange with the surroundings.

As regards the HPT pressure, the values found for each tank always respect the limit imposed by the protocol.

4.1.3. Low pressure tanks results

As previously explained, the LPT refuels, whenever its SOC is less than 100%, with a mass flow rate equal to that of HG production (13.89 g/s). Simultaneously, it empties when required by the HPT cascade system (−60 g/s). Following the logic imposed, when the SOC equals 100%, the LPT is not filled, but only emptied when required. Instead, in the case where the SOC is below 100% and there is a request from the HPTs, the LPT empties by the difference between the compressed flow rate and that produced by the HG (close to −46 g/s). Finally, in moments when there is no hydrogen demand downstream and when the VTs and HPTs have already reached an SOC of 100%, the LPT fills.

The pressure presents a trend analogous to that of the SOC, as previously seen by the other tanks. The initial value starts from the nominal pressure value, 3.5 MPa, equal to the hydrogen production pressure by the HG.

Regarding temperatures, since the LPT is mainly characterized by emptying phases, the gas temperature decreases from ambient temperature down to a minimum of −19.43°C, then increases in the final filling phase with hydrogen arriving from the HG at 55°C. The wall temperature instead remains almost constant, with a slight decrease visible at the end. This phenomenon is primarily due to the significant larger volume of the LPT tank (150 m^3) compared to the HPTs (1.25-1.75 m^3) and VT (0.27 m^3), which provides substantial thermal mass and inertia. Additionally, the Type I steel construction (thermal conductivity of 50 W/mK) facilitates continuous heat exchange with the ambient environment, maintaining wall temperature close to ambient conditions despite gas temperature fluctuations.

4.2. Parametric analysis result

This section reports the results of the parametric analysis, varying one or more parameters, with the objective of identifying the maximum number of full refueling that the HRS considered in this study is theoretically capable of guaranteeing. Some of the input parameter values presented in Table 8 were varied (less the initial SOCs) to find a number of refueling greater than 5, initially hypothesized.

The first parameters to be varied were the APRR (between 4.5 MPa/min and 9.5 MPa/min) and the compressed hydrogen mass flow rate (between 60 g/s and 120 g/s). After identifying a baseline APRR value ensuring compliance with the target constraints (4.5 MPa/min), the APRR value was increased to evaluate the sensitivity of the system performance and to assess the potential increase in the number of refuelings while maintaining protocol constraints. The selection of these two parameters is partly dictated by the system logic. To increase the number of refueling, the APRR is adjusted, which increases the hydrogen flow rate required from the storage system. However, to ensure that the cascade system maintains a sufficient SOC during each refueling, it is also necessary to increase the compression flow rate upstream of the cascade system itself. Through a parametric analysis varying the two aforementioned parameters, the minimum compression flow rate was determined to guarantee the required number of refueling, initially set at 5, for each APRR considered. Subsequently, with the objective of increasing the number of refueling, an analogous parametric analysis was performed for target values of 6, 7, and 8 refueling. The results are presented in Fig. 8. Only the operating points satisfying all the imposed constraints are reported on the curves. In particular, the plotted points simultaneously fulfil the target number of refuelings within the hour, the SAE temperature limits, the minimum allowable LPT pressure, and a final cascade system SOC equal to 100%.

As can be observed, with increasing number of refuelings, the curves shift toward higher compressed hydrogen flow rates (rightward), while the number of points on the curves decreases. Indeed, in the case of 7 refuelings, an APRR of 4.5 MPa/min never satisfies the target number of refuelings within the hour, whereas a value of 9.5 MPa/min consistently exceeds the temperature limit in HPT3. For 8 refuelings, both an APRR of 4.5 MPa/min and 5.5 MPa/min fail to satisfy the number of refuelings, while again at 9.5 MPa/min the temperature limit in HPT3 is exceeded and the LPT pressure drops below the minimum allowable value (1.5 MPa). The regions located on the left-hand side of each curve correspond to operating conditions for which at least one constraint is not satisfied. More specifically, for the case of 5 refuelings, the only unmet requirement at lower compressed hydrogen flow rates is the target number of refuelings. For 6, 7, and 8 refuelings, lower flow rates also lead to violation of the maximum temperature limit in HPT3 (85°C according to the SAE protocol). In addition, for the case of 8 refuelings, the minimum allowable LPT pressure is not satisfied at low APRR values. The results and the limiting conditions are summarized in Table 10.

To address the temperature issue, the same parametric analysis was performed with a cascade system volume increased by 30% compared to the initial value. The results are presented in Fig. 9. As can be observed, compared to the previous case, some of the obtained values are now

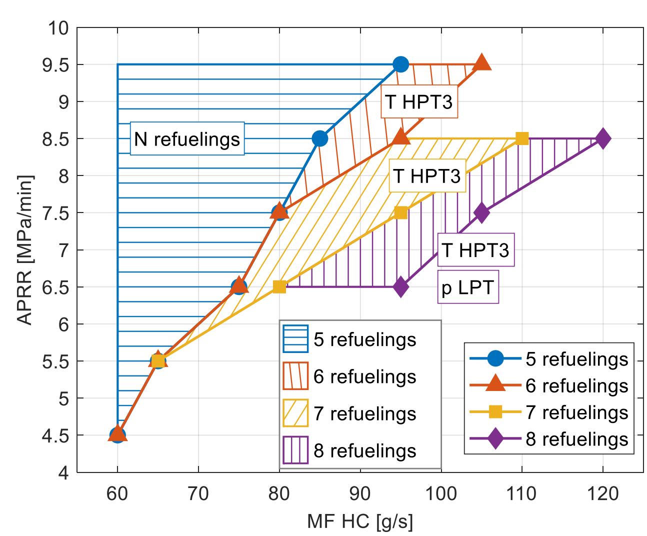

Fig. 8. Parametric analysis by varying APRR, mass flow HC and number of refuelings.

Table 10
Results obtained after the first parametric analysis.

N° Refuelings	Feasible APRR range [MPa/min]	Minimum H2 Flow Rate [g/s]	Limiting constrain (Lower APRR or flow rate)
5	4.5 – 9.5	60 – 95	Refueling target
6	4.5 – 9.5	60 – 105	HPT3 Temperature
7	5.5 – 8.5	80 – 110	HPT3 Temperature
8	6.5 – 8.5	95 – 120	HPT3 Temperature and LPT Pressure

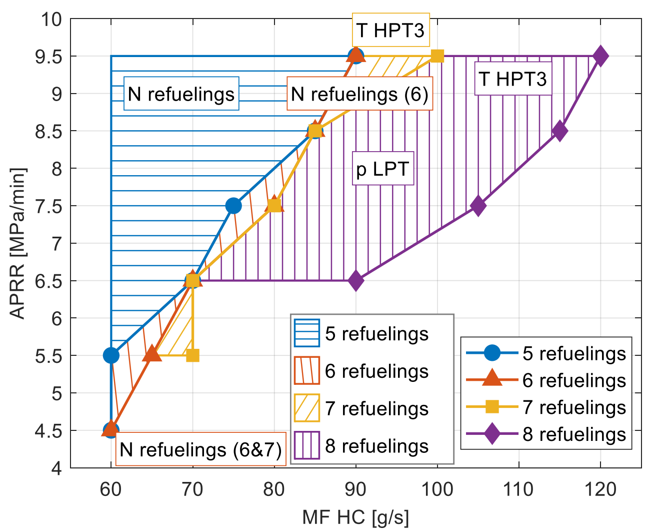

Fig. 9. Parametric analysis by varying APRR, mass flow HC, number of refuelings and cascade system volume by 30%.

shifted leftward. This is due to the fact that by increasing the cascade system volume, which is characterized by an initial SOC of 100%, a lower compression flow rate is required thanks to the greater initial hydrogen quantity.

Only the operating points satisfying all the imposed constraints are reported on the curves. The points corresponding to APRR values that do not satisfy the target number of refuelings for the cases of 7 and 8 refuelings (i.e., 4.5 MPa/min and 5.5 MPa/min) are not shown in the figure. Conversely, the points characterized by an APRR of 9.5 MPa/min, which were absent in the previous case, now satisfy the temperature and pressure constraints.

The regions located on the left-hand side of each curve correspond to operating conditions for which at least one of the target constraints is not satisfied. In these regions, the most frequently violated constraint at lower compressed hydrogen flow rates is the target number of refuelings, particularly for the cases of 5, 6, and 7 refuelings. Furthermore, for 7 and 8 refuelings, the HPT3 temperature constraint is exceeded at high APRR values. Finally, in the case of 8 refuelings and lower compressed hydrogen flow rates, the minimum allowable LPT pressure is never satisfied. Thes summarized results are shown in Table 11.

Table 11
Results obtained after the second parametric analysis.

N° Refuelings	Feasible APRR range [MPa/min]	Minimum H2 Flow Rate [g/s]	Limiting constrain (Lower APRR or flow rate)
5	4.5 – 9.5	60 – 90	Refueling target
6	4.5 – 9.5	60 – 90	Refueling target
7	5.5 – 9.5	70 – 100	Refueling target and HPT3 Temperature
8	6.5 – 9.5	90 – 120	HPT3 Temperature and LPT Pressure

To ensure compliance with the temperature constraint even at high APRR values, a final parametric analysis was performed, this time considering a 45% increase in the cascade system volume compared to the initial value. The results are presented in Fig. 10. As previously observed, the minimum compressed flow rate values obtained are partially shifted leftward. As before, only the operating points satisfying all the imposed constraints are reported on the curves.

Considering lower flow rates (the regions located on the left-hand side of each curve), the least satisfied parameter remains the target number of refuelings, while the temperature values are now always satisfied. Another parameter that is not satisfied at lower flow rates is the LPT pressure in the case of 8 refuelings. In this regard, the LPT volume could be increased; however, since the hydrogen production flow rate and consequently the hydrogen stored in the LPT will be optimized subsequently, it was decided to maintain a constant tank volume at this stage. A final consideration concerns the minimum flow rates obtained for an APRR of 4.5 MPa/min (6 refuelings) and 5.5 MPa/min (7 refuelings). These points exhibit a minimum flow rate higher than that obtained for the immediately subsequent APRR: for 6 refuelings, a flow rate of 65 g/s is required at 4.5 MPa/min compared to 60 g/s at 5.5 MPa/min, while for 7 refuelings, a flow rate of 75 g/s was found at 5.5 MPa/min versus 70 g/s at 6.5 MPa/min. This aspect is primarily related to the final refilling of the cascade system (rather than to the refueling of the VTs), which must be completed within the hour: to ensure this is possible, it was necessary to increase the compression flow rate. The results are reported in Table 12.

In summary, the parametric analysis varying one or more parameters showed satisfactory results, regarding the number of refuelings guaranteed, for either 6, 7 or 8 refuelings in 1 h. This approach allows the identification of operating conditions that improve system performance (in terms of number of refuelings) while ensuring compliance with all constraints and limiting energy consumption.

Regarding the HRS components, major problems occurred with HPT3: these were remedied by increasing the volume of the cascade system, in cases where HPT3 temperature exceeded the limit of 85°C. The LPT also contributed to the failure of some simulations, but only for those characterized by a high number of refuelings and a high compressed flow rate.

Of the initial inputs, it was decided not to vary all parameters. As said before, the LPT volume was kept constant in all simulations during this phase, as it does not affect the achievement of the target number of refuelings. The hydrogen production mass flow rate was also kept constant: in fact, it was calculated to satisfy the required refuelings and to

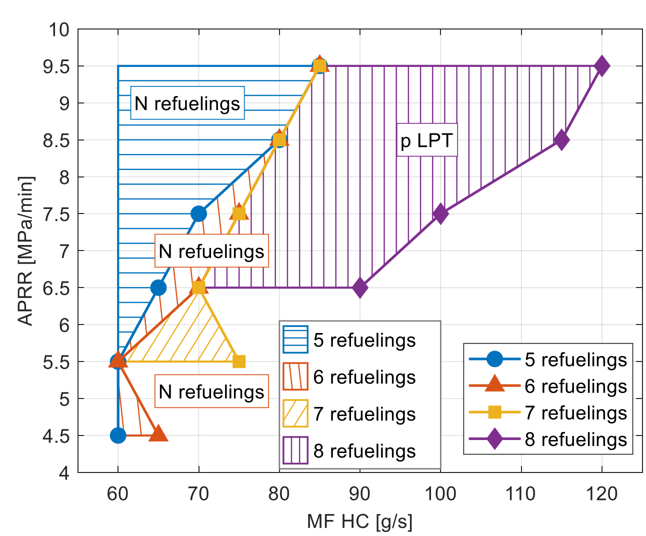

Fig. 10. Parametric analysis by varying APRR, mass flow HC, number of refuelings and cascade system volume by 45%.

Table 12
Results obtained after the final parametric analysis.

N° Refuelings	Feasible APRR range [MPa/min]	Minimum H2 Flow Rate [g/s]	Limiting constrain (Lower APRR or flow rate)
5	4.5 – 9.5	60 – 85	Refueling target
6	4.5 – 9.5	60 – 85	Refueling target
7	5.5 – 9.5	70 – 85	Refueling target
8	6.5 – 9.5	90 – 120	LPT Pressure

refuel the LPT throughout the day. Furthermore, the solution with a production of approximately 15 g/s of hydrogen is already energy-intensive, and not suitable in the case where vehicles are to be refuelled with green hydrogen, as the electrolyzer would run most of the day to refuel the LPT. This aspect will therefore be improved subsequently. Also, the precooling temperature was left constant and equal to −10°C: this temperature, in fact, influences only the gas temperature inside the VTs, already under control with the selected ambient temperature. Like the PC temperature, the ambient temperature was left constant, considering this temperature as average throughout the year. This choice can be acceptable for the theoretical functioning of HRS operation and will be further investigated subsequently. Finally, additional tests were not performed, as the results obtained for the satisfactory tests were close to the temperature or pressure limits or would almost certainly have increased consumption.

Regarding the results of the satisfactory tests just analysed, as explained, the number of refuelings is the same as the target. The refueling time is strictly related to the maximum hydrogen flow rate delivered by the dispenser: indeed, the shorter the refueling time, the higher the hydrogen flow rate, which is influenced by the APRR value. The shortest times were obtained, for obvious reasons, with higher APRR values and range overall between 3.45 min (APRR = 9.5 MPa/min) and 7.15 min (APRR = 4.5 MPa/min). These values correspond to the highest delivered flow rate, approximately 180.62 g/s, and the lowest, 83.26 g/s.

As for the pressure, the tank characterized by a value close to the limit is HPT3, followed by HPT2, VT and HPT1. As previously highlighted, HPT3 is indeed the most stressed tank during refueling, according to the established priority logic. For the LPT, conversely, the values found tend more toward the lower limit. Regarding temperature, the tank characterized by values close to the limit of 85°C is HPT3, now followed by HPT2 and the VT. Lower temperatures are found in HPT1, which is last in the cascade system management logic, and the LPT, which predominantly undergoes emptying phases that do not increase temperature. As for pressure, the results do not vary visibly from one test to another, except for the LPT, which presents a more or less marked decrease in results (with the end values comprises between −20°C ÷ −55°C).

The low temperatures observed in the LPT are associated with hydrogen expansion during tank emptying, leading to a temperature decrease consistent with the thermodynamic behaviour of the gas. While the present model focuses on system-level performance, such conditions should be taken into account in practical applications through appropriate engineering design.

Regarding the SOC values, the tank that is emptied the most is HPT3, as established by the logic. Consequently, HPT2 is less depleted, while HPT1 has values close to 100%.

Finally, the highest power required by the compressor was found for higher compressed flow rates (120 g/s), while the highest value of PC power is due to the higher APRR value considered (9.5 MPa/min), while higher power does not correspond to higher consumption. Furthermore, the PC power is between 6.74% ÷ 8.25% of the HC power, while at the consumption level the percentage decreases 3.62% ÷ 4.6%. In general, among the different tests (or the points in 8, 9 and 10), there is no evident change between the results found.

Overall, the performed parametric analyses also provide an indirect assessment of the sensitivity of the HRS performance to the main operating parameters. Variations of APRR, compression mass flow rate, and cascade storage volume allowed evaluating the robustness of the model predictions and identifying the parameters having the greatest influence on the achievable number of refuelings and on temperature and pressure constraints. The results show that the general trends and system behaviour remain consistent over a relatively wide range of operating conditions. Furthermore, as discussed in Section 2, neglected hydraulic losses and short-duration valve-switching transients are expected to have a limited impact on the global performance indicators considered in this work. A rigorous uncertainty propagation analysis was considered beyond the scope of the present study and will be addressed in future developments.

Furthermore, the low temperatures observed in the LPT (down to approximately −55°C) suggest that future work should investigate material compatibility and structural integrity under cryogenic-like operating conditions, as well as possible mitigation strategies such as thermal insulation or auxiliary heating systems to ensure safe and reliable operation.

5. Conclusions

In this study, the development of a mathematical and thermodynamic model of a 35 MPa HRS was designed. The model, implemented in MATLAB-Simulink, integrates all main station components, or LPT, HC, HPT cascade system, PC, and VTs.

A comprehensive thermodynamic analysis of critical parameters (hydrogen mass flow rate, pressure, temperature) was conducted for each system component. A parametric analysis was then performed to identify optimal initial conditions maximizing the number of consecutive refueling, starting from initially empty vehicles (VT SOC = 10%). Favourable configurations were identified for 5, 6, 7, and 8 consecutive refueling. Results demonstrated that pressure and temperature remain consistently below the limits imposed by the SAE J2601-5 protocol, with minimum energy consumption for 6 refueling and refueling times ranging from 3.45 to 7.15 min.

Overall, the results demonstrate that the proposed control logic for the cascade system, combined with precooling of the supplied hydrogen (−10°C), enables safe and efficient HRS operation under variable demand conditions. However, winter operation requires additional thermal management strategies, such as extended idle periods or strategic tank rotation, to prevent long-term heat accumulation and ensure sustained compliance with temperature limits. The validated model provides a flexible tool for adapting station design and control strategies to different seasonal and operational scenarios.

Beyond confirming expected trends associated with cascade storage and thermal management, the proposed model provides a system-level framework for identifying feasible operating regions and for evaluating the interactions among APRR, compressor capacity, and cascade storage volume under heavy-duty refueling conditions. The parametric analysis showed that the limiting factors governing station throughput are not fixed, but depend on the combined effects of temperature constraints in HPT3 and minimum pressure requirements in the LPT. Therefore, the model can support the design and sizing of HRS components and operating strategies for different demand scenarios, providing practical guidelines for heavy-duty hydrogen refueling applications.

Furthermore, the low temperatures observed in the LPT during intense emptying phases suggest that future work should investigate material compatibility and possible mitigation strategies, such as thermal insulation or auxiliary heating, to ensure reliable operation under low-temperature conditions.

The next steps of the study concern: 1) the integration of the analysed HRS into a renewable energy-based microgrid, considering different energy management strategies; 2) the microgrid model optimization, to determine the optimal component sizing for two objective functions:

maximizing the Self-Sufficiency Ratio and minimizing the Levelized Cost of Hydrogen; 3) a comprehensive cost analysis, considering both the revenue from surplus electricity sales and the expected decrease in Hydrogen Generator costs in the coming years; 4) the calculation of the avoided CO_2 emissions for each EMS, including both emissions from Fuel Cell Electric Vehicle operation and those related to the renewable electricity powering the electrolyzer and HRS components.

CRediT authorship contribution statement

Roberta Tatti: Conceptualization, Data curation, Formal analysis, Investigation, Methodology, Software, Validation, Visualization, Writing – original draft, Writing – review & editing. **Mario Petrollese:** Conceptualization, Formal analysis, Supervision, Visualization, Writing – review & editing.

Declaration of competing interest

The authors declare that they have no known competing financial interests or personal relationships that could have appeared to influence the work reported in this paper.

References

[1] Filonchyk M, Peterson MP, Yan H, Gusev A, Zhang L, He Y, et al. Greenhouse gas emissions and reduction strategies for the world's largest greenhouse gas emitters. Sci Total Environ 2024;944:173895. https://doi.org/10.1016/J.SCITOTENV.2024.173895.

[2] Gürbüz H. Analysis of the operating characteristics of hydrogen PEM fuel cell and battery onelectric vehicle in different driving cycles. Environ Prog Sustain Energy 2023;42:e14146. https://doi.org/10.1002/EP.14146.

[3] Pergamalis C, Tsampasis E, Dedes IC, Elias C. Hydrogen fuel cell electrical vehicles (FCEV) - Battery electric vehicles (BEV) - comparison and future challenges. In: 2024 13th mediterranean conference on embedded computing, MECO; 2024. https://doi.org/10.1109/MECO62516.2024.10577907. 2024.

[4] Aguilar PA, Groß B. Battery electric vehicles and fuel cell electric vehicles, an analysis of alternative powertrains as a mean to decarbonise the transport sector. SSRN Electron J 2022. https://doi.org/10.2139/SSRN.4112184.

[5] Endiz MS. A comparison of battery and hydrogen fuel cell electric vehicles for clean transportation. Orclever Proceed Res Dev 2023;2:10–7. https://doi.org/10.56038/OPRD.V2I1.230.

[6] International Energy Agency. Global hydrogen review 2024. https://iea.blob.core.windows.net/assets/89c1e382-dc59-46ca-aa47-9f7d41531ab5/GlobalHydrogenReview2024.pdf. [Accessed 21 July 2025].

[7] International Energy Agency. Global electric vehicles outlook. https://iea.blob.core.windows.net/assets/7ea38b60-3033-42a6-9589-71134f4229f4/GlobalEVOutlook2025.pdf. [Accessed 21 July 2025].

[8] Rivard E, Trudeau M, Zaghib K. Hydrogen storage for mobility: a review. Materials 2019;12. https://doi.org/10.3390/MA12121973. Page 1973 2019;12:1973.

[9] Mulky L, Srivastava S, Lakshmi T, Sandadi ER, Gour S, Thomas NA, et al. An overview of hydrogen storage technologies – key challenges and opportunities. Mater Chem Phys 2024;325:129710. https://doi.org/10.1016/J.MATCHEMPHYS.2024.129710.

[10] Ni M. An overview of hydrogen storage technologies. Energy Explor Exploit 2006;24:197–209. https://doi.org/10.1260/014459806779367455;REQUESTEDJOURNAL:JOURNAL:EEAA.

[11] Mehr AS, Phillips AD, Brandon MP, Pryce MT, Carton JG. Recent challenges and development of technical and technoeconomic aspects for hydrogen storage, insights at different scales; A state of art review. Int J Hydrogen Energy 2024;70:786–815. https://doi.org/10.1016/J.IJHYDENE.2024.05.182.

[12] Bosu S, Rajamohan N. Recent advancements in hydrogen storage - comparative review on methods, operating conditions and challenges. Int J Hydrogen Energy 2024;52:352–70. https://doi.org/10.1016/J.IJHYDENE.2023.01.344.

[13] Wang Q, Li J, Bu Y, Xu L, Ding Y, Hu Z, et al. Technical assessment and feasibility validation of liquid hydrogen storage and supply system for heavy-duty fuel cell truck. 2020 4th CAA international conference on vehicular control and intelligence. CVCI; 2020 2020. p. 555–60. https://doi.org/10.1109/CVCI51460.2020.9338639.

[14] Austin R, Baird EH, Brian D, Ehrhart AM. Liquid hydrogen heavy-duty vehicle safety review and refueling facility design. Sandia Report 2022. https://www.osti.gov/servlets/purl/1885100/. [Accessed 23 August 2025].

[15] Ahluwalia RK, Roh HS, Peng JK, Papadias D, Baird AR, Hecht ES, et al. Liquid hydrogen storage system for heavy duty trucks: configuration, performance, cost, and safety. Int J Hydrogen Energy 2023;48:13308–23. https://doi.org/10.1016/J.IJHYDENE.2022.12.152.

[16] Ahluwalia RK, Peng JK, Roh HS, Papadias D, Wang X, Aceves SM. Liquid hydrogen storage system for heavy duty trucks: capacity, dormancy, refueling, and discharge. Int J Hydrogen Energy 2023;48:34120–31. https://doi.org/10.1016/J.IJHYDENE.2023.05.113.

[17] Mark D, Allendorf RH. Assessment of tank designs for hydrogen storage on heavy duty vehicles using metal hydrides. Sandia Report; 2023.

[18] Alenezi M, Alarbeed B, Alqaheem Y. Metal hydrides and metal-organic frameworks for hydrogen storage in automotive applications: A review n.d. https://doi.org/10.32737/2221-8688-2024-1-76-94.

[19] Parashar S, Muthukumar P, Kumar Soti A. Experimental study on absorption and desorption behavior of a novel metal hydride reactor for stationary hydrogen storage applications. Int J Hydrogen Energy 2024;94:1224–35. https://doi.org/10.1016/j.ijhydene.2024.11.058.

[20] Couteau A, Dimopoulos Eggenschwiler P, Jenny P. Heat transfer analysis of high pressure hydrogen tank fillings. Int J Hydrogen Energy 2022;47:23060–9. https://doi.org/10.1016/J.IJHYDENE.2022.05.127.

[21] Oh SJ, Yoon JH, Jeon KS, Choi JJ. A numerical study on characteristics of heat transfer in hydrogen filling storage vessel by charging conditions. Int J Hydrogen Energy 2022;47:25679–95. https://doi.org/10.1016/J.IJHYDENE.2022.05.306.

[22] Li JQ, Chen Y, Ma YB, Kwon JT, Xu H, Li JC. A study on the Joule-Thomson effect of during filling hydrogen in high pressure tank. Case Stud Therm Eng 2023;41:102678. https://doi.org/10.1016/J.CSITE.2022.102678.

[23] Fragiacomo P, Martorelli M, Genovese M, Piraino F, Corigliano O. Thermodynamic modelling, testing and sensitive analysis of a directly pressurized hydrogen refueling process with a compressor. Renew Energy 2024;226:120410. https://doi.org/10.1016/J.RENENE.2024.120410.

[24] Sgaramella A, Lo Basso G, de Santoli L. How the cylinder initial conditions affect the HCNG refueling process - a thermodynamic analysis to determine the most effective filling parameters. Int J Hydrogen Energy 2024;51:559–75. https://doi.org/10.1016/J.IJHYDENE.2023.07.323.

[25] Sapre S, Pareek K, Vyas M. Investigation of structural stability of type IV compressed hydrogen storage tank during refueling of fuel cell vehicle. Energy Storage 2020;2:e150. https://doi.org/10.1002/EST2.150.

[26] Sapre S, Vyas M, Pareek K. Impact of refueling parameters on storage density of compressed hydrogen storage tank. Int J Hydrogen Energy 2021;46:16685–92. https://doi.org/10.1016/J.IJHYDENE.2020.08.136.

[27] High-flow prescriptive fueling protocols for gaseous hydrogen powered medium and heavy-duty vehicles. SAE J2601/5_202402 2024. https://doi.org/10.4271/J2601/5_202402.

[28] De Miguel N, Ortiz Cebolla R, Acosta B, Moretto P, Harskamp F, Bonato C. Compressed hydrogen tanks for on-board application: thermal behaviour during cycling. Int J Hydrogen Energy 2015;40:6449–58. https://doi.org/10.1016/J.IJHYDENE.2015.03.035.

[29] Molkov V, Dadashzadeh M, Makarov D. Physical model of onboard hydrogen storage tank thermal behaviour during fuelling. Int J Hydrogen Energy 2019;44:4374–84. https://doi.org/10.1016/J.IJHYDENE.2018.12.115.

[30] Deng S, Xiao J, Bénard P, Chahine R. Determining correlations between final hydrogen temperature and refueling parameters from experimental and numerical data. Int J Hydrogen Energy 2020;45:20525–34. https://doi.org/10.1016/J.IJHYDENE.2019.12.225.

[31] Liu J, Zheng S, Zhang Z, Zheng J, Zhao Y. Numerical study on the fast filling of on-bus gaseous hydrogen storage cylinder. Int J Hydrogen Energy 2020;45:9241–51. https://doi.org/10.1016/J.IJHYDENE.2020.01.033.

[32] Fragiacomo P, Martorelli M, Genovese M. Numerical modeling for analysis and improvement of hydrogen refueling process for heavy-duty vehicles. Appl Energy 2025;380:125092. https://doi.org/10.1016/J.APENERGY.2024.125092.

[33] Luo H, Xiao J, Bénard P, Yuan C, Tong L, Chahine R, et al. Thermodynamic modeling and analysis of cascade hydrogen refueling with three-stage pressure and temperature for heavy-duty fuel cell vehicles. Int J Hydrogen Energy 2024;63:103–13. https://doi.org/10.1016/J.IJHYDENE.2024.03.060.

[34] Xiao J, Xu N, Cai W, Zhou X, Bénard P, Chahine R, et al. Thermodynamic and heat transfer models for refueling hydrogen vehicles: formulation, validation and application. Int J Hydrogen Energy 2024;52:172–90. https://doi.org/10.1016/J.IJHYDENE.2023.06.081.

[35] Tun H, Reddi K, Elgowainy A, Poudel S. Thermodynamic parametric analysis of refueling heavy-duty hydrogen fuel-cell electric vehicles. Int J Hydrogen Energy 2023;48:28869–81. https://doi.org/10.1016/J.IJHYDENE.2023.04.075.

[36] Stops L, Siebe D, Stary A, Hamacher J, Sidarava V, Rehfeldt S, et al. Generalized thermodynamic modeling of hydrogen storage tanks for truck application. Cryogenics 2024;139:103826. https://doi.org/10.1016/J.CRYOGENICS.2024.103826.

[37] Saferna A, Saferna P, Kuczyński S, Łaciak M, Szurlej A, Włodek T. Effects of hydrogen, methane, and their blends on rapid-filling process of high-pressure composite tank. Energies 2024:1130. https://doi.org/10.3390/EN17051130. Vol 17, Page 1130 2024;17.

[38] Caponi R, Ferrario AM, Bocci E, Bødker S, del Zotto L. Single-tank storage versus multi-tank cascade system in hydrogen refueling stations for fuel cell buses. Int J Hydrogen Energy 2022;47:27633–45. https://doi.org/10.1016/J.IJHYDENE.2022.06.100.

[39] Galassi MC, Baraldi D, Acosta Iborra B, Moretto P. CFD analysis of fast filling scenarios for 70 MPa hydrogen type IV tanks. Int J Hydrogen Energy 2012;37:6886–92. https://doi.org/10.1016/J.IJHYDENE.2012.01.041.

[40] Li JQ, Li JCL, Park K, Kwon JT. Investigation on the changes of pressure and temperature in high pressure filling of hydrogen storage tank. Case Stud Therm Eng 2022;37:102143. https://doi.org/10.1016/J.CSITE.2022.102143.

[41] Hall C, Ramasamy V. Modelling the conjugate heat transfer during the fast-filling of high-pressure hydrogen vessels for vehicular transport. Int J Thermofluids 2024;21:100527. https://doi.org/10.1016/J.IJFT.2023.100527.

[42] Genovese M, Fragiacomo P. Hydrogen refueling station: overview of the technological status and research enhancement. J Energy Storage 2023;61:106758. https://doi.org/10.1016/J.EST.2023.106758.
[43] Caponi Roberta, Ferrario Andrea Monforti, Bocci Enrico, Valenti Gianluca, Della Pietra Massimiliano. Thermodynamic modeling of hydrogen refueling for heavy-duty fuel cell buses and comparison with aggregated real data. Int J Hydrogen Energy 2021;46(35):18630–43. https://doi.org/10.1016/j.ijhydene.2021.02.224. ISSN 0360-3199.
[44] Ruffio Emmanuel, Saury Didier, Petit Daniel. Thermodynamic analysis of hydrogen tank filling. Effects of heat losses and filling rate optimization. Int J Hydrogen Energy 2014;39(24):12701–14. https://doi.org/10.1016/j.ijhydene.2014.06.069. ISSN 0360-3199.
[45] Li Ji-Qiang, Li Ji-Chao, Wang Xiang-Yang, Xu Heng, Kwon Jeong-Tae, Leng ChengLin. A numerical study on the thermal behavior of high pressure hydrogen in the on-board storage cylinder. AIP Adv 2023;13(7):075222. https://doi.org/10.1063/5.0143732.
[46] Tatti R, Klopčič N, Radner F, Petrollese M. Thermodynamic modelling and analysis of A hydrogen refueling station using Matlab-Simulink. In: 38th International Conference On Efficiency, Cost, Optimization, Simulation And Environmental Impact Of Energy Systems (ECOS)), 29; 2025.
[47] Bourgeois T, Ammouri F, Baraldi D, Moretto P. The temperature evolution in compressed gas filling processes: a review. Int J Hydrogen Energy 2018;43: 2268–92. https://doi.org/10.1016/J.IJHYDENE.2017.11.068.
[48] Klopčič N, Regenfelder R, Hafner T, Winkler F, Rasche C, Rink M, et al. Refueling tests of a hydrogen tank for heavy-duty applications. Int J Hydrogen Energy 2024; 49:1237–49. https://doi.org/10.1016/J.IJHYDENE.2023.09.109.
[49] Baglioni Group. Hydrogen - Baglioni group products n.d. https://baglionispa.com/en/hydrogen. [Accessed 8 September 2025].
[50] Safra Group. HYCITY ® : hydrogen bus - safra n.d. https://safra.fr/en/hycity-2/. [Accessed 3 September 2025].
[51] Rothuizen E, Rokni M. Optimization of the overall energy consumption in cascade fueling stations for hydrogen vehicles. Int J Hydrogen Energy 2014;39:582–92. https://doi.org/10.1016/J.IJHYDENE.2013.10.066.
[52] Xiao L, Chen J, Wu Y, Zhang W, Ye J, Shao S, et al. Effects of pressure levels in three-cascade storage system on the overall energy consumption in the hydrogen refueling station. Int J Hydrogen Energy 2021;46:31334–45. https://doi.org/10.1016/J.IJHYDENE.2021.07.007.
[53] Manoharan Y, Hosseini SE, Butler B, Alzhahrani H, Senior BTF, Ashuri T, et al. Hydrogen fuel cell vehicles; current status and future prospect. Appl Sci 2019;9: 2296. https://doi.org/10.3390/APP9112296. 2019;9:2296.
[54] American Petroleum Institute. Reciprocating compressors for petroleum, Chemical, and Gas Industry Services. section 6.5.1, https://www.apiwebstore.org/standards/618; 2007 (accessed September 8, 2025).
[55] Smith R. Chemical process - design and integration. https://archive.org/details/chemicalprocessd0000smit_f5r6. [Accessed 8 September 2025].
[56] Poudel S, Tun H, Reddi K, Elgowainy A. Investigation of precooling unit design options in hydrogen refueling station for heavy-duty fuel-cell electric vehicles. Int J Hydrogen Energy 2024;61:493–502. https://doi.org/10.1016/J.IJHYDENE.2024.02.197.
[57] Reddi A, Elgowainy A, Rustagi N, Gupta E. Impact of hydrogen refueling configurations and market parameters on the refueling cost of hydrogen. J Power Sources 2017;360:511–21. https://doi.org/10.1016/j.jpowsour.2017.05.100.
[58] Moradi M, Groth K. Hydrogen storage and delivery: review of the state of the art technologies and risk and reliability analysis. Int J Hydrogen Energy 2019;44(23): 12254–69. https://doi.org/10.1016/j.ijhydene.2019.03.041.
[59] Zhang, J, et al. Energy analysis and optimization of hydrogen refueling stations *energies*, 16(3), 2023, 1234. https://doi.org/10.3390/en16031234.